A Two-Element Antenna for Null Suppression in Multipath Environments

William F. Young, Benjamin Belzer, *Member, IEEE,* and Robert G. Olsen, *Fellow, IEEE*

***Abstract*—The design of a two-element antenna for portable transceivers is considered. The antenna consists of a dipole terminated with a parallel loop-capacitor combination. The antenna has a single feed at a point on the loop opposite the junction and does not require external combining circuitry. The capacitor creates a phase shift between the dipole and loop currents, thereby greatly reducing the probability of deep nulls in the received signal when the antenna is deployed in free-space or in the vicinity of a fixed reflector, where standing wave patterns occur. Theoretical and simulation studies based on multiple incident/reflected plane wave fields typical of multipath environments are used to quantify the reduction in null probability. Simulation results are presented for three antenna types: a dipole antenna, a loop-dipole antenna without a capacitor, and the loop-dipole antenna with capacitor. The results are verified by field measurements on an automated outdoor test range, where the incidence angle and distance from the reflector are varied. With a single incident plane wave, the loop-dipole-capacitor (LDC) design reduces the probability of deep nulls in the received signal by up to two orders of magnitude at low signal-to-noise ratios (SNRs) when compared with the standard dipole antenna and the loop-dipole antenna without the capacitor. The performance advantage of the new design decreases as the number of incident waves increases; however, it performs at least as well as the dipole antenna in all cases studied.**

***Index Terms*—Antenna measurements, mobile antennas, multipath channels, wire antennas.**

I. Introduction and Background

THIS paper describes the design and performance of a two element antenna intended for portable transceivers. It is assumed that the antenna is operated in an electromagnetic field consisting of one or more incident/reflected wave pairs such as are commonly found in urban environments near planar reflecting surfaces (e.g., external walls of buildings). The resulting field pattern can either be responsible for deep fades, or exploited by antennas such as the one discussed here. The antenna is designed to reduce the probability of deep nulls in the received signal, compared to a dipole antenna, when used over a wide range of field polarization and incidence angles, and over a range of antenna positions relative to a fixed reflector. Combining of the colocated antenna elements is realized through the use of passive components so that no special signal processing electronics are needed to use the antenna and so that the antenna has a single feedpoint. The antenna, therefore, can be made plug-in compatible with preexisting portable communication devices, without the need for additional electrical interfaces or circuitry other than a simple matching network. The design has potential practical application as a plug-in replacement for the monopole antennas typically provided by transceiver manufacturers.

The antenna configuration studied in this paper is shown in Fig. 1. The loop and dipole elements respond to the E_a and H_a and field components, respectively, where the a-axis is aligned along the dipole (Fig. 2). For electrically small antenna elements, the loop and dipole are effectively combined in series so that the antenna output voltage magnitude is

$$V = |v_D + v_L| = C\left|E_a + \eta_0 e^{j(\gamma+\pi/2)} H_a\right|. \quad (1)$$

In this equation, C is a gain constant having units of length, η_0 is the impedance of free-space, γ is the extra phase introduced between the loop and dipole contributions by the capacitor, and the antenna geometry has been adjusted to provide equal dipole and loop voltage magnitudes when $H_a = E_a/\eta_0$.

The motivation for a two-element antenna will be discussed next. Consider a single plane wave propagating along the x-axis with a z-oriented electric field of amplitude E_0. The axis a of the two-element antenna is in the yz-plane tilted at an angle θ_a with respect to the z-axis. Thus, the field components along the a-axis are $E_a = E_0\cos(\theta_a)$ and $H_a = (E_0/\eta_0)\sin(\theta_a)$. If $\gamma = 0$ (i.e., no capacitor), the antenna output voltage according to (1) is $V = CE_0$, which is independent of the antenna tilt angle θ_a as well as being independent of position along the x-axis. This property is the reason why such a two-element antenna is desirable. Note however, that setting $\gamma = \pi/2$ gives $V = CE_0|\cos(\theta_a) - \sin(\theta_a)|$, which produces a null at $\theta_a = \pi/4$.

If however, the antenna is placed in front of a perfect reflecting plane with normal along the x-axis, the fields become $E_a = -2jE_0\cos(\theta_a)\sin(k_0 d)$ and $H_a = -2(E_0/\eta_0)\sin(\theta_a)\cos(k_0 d)$, respectively, where k_0 is the propagation constant and d is the distance from the reflector. If $\gamma = 0$, the antenna output voltage is $V = 2CE_0|\cos(\theta_a)\sin(k_0 d) + \sin(\theta_a)\cos(k_0 d)|$, which is zero for certain values of θ_a and periodic distances from the reflector. If a capacitor is introduced and $\gamma = \pi/2$, the two contributions add in quadrature and the antenna output voltage is

$$V = 2CE_0[\cos^2(\theta_a)\sin^2(k_0 d) + \sin^2(\theta_a)\cos^2(k_0 d)]^{1/2} \quad (2)$$

and the nulls disappear.

It appears that nulls can be suppressed under both conditions (with and without reflector) by choosing a value of γ close to

Manuscript received April 6, 1998; revised March 20, 2000. This work was supported by grants from the Washington Technology Center and Larsen Electronics, Inc., and by The Boeing Company Distinguished Professorship in Electrical Engineering.

The authors are with the School of Electrical Engineering and Computer Science, Washington State University, Pullman, WA 99164-2752 USA.

Publisher Item Identifier S 0018-926X(00)07709-7.

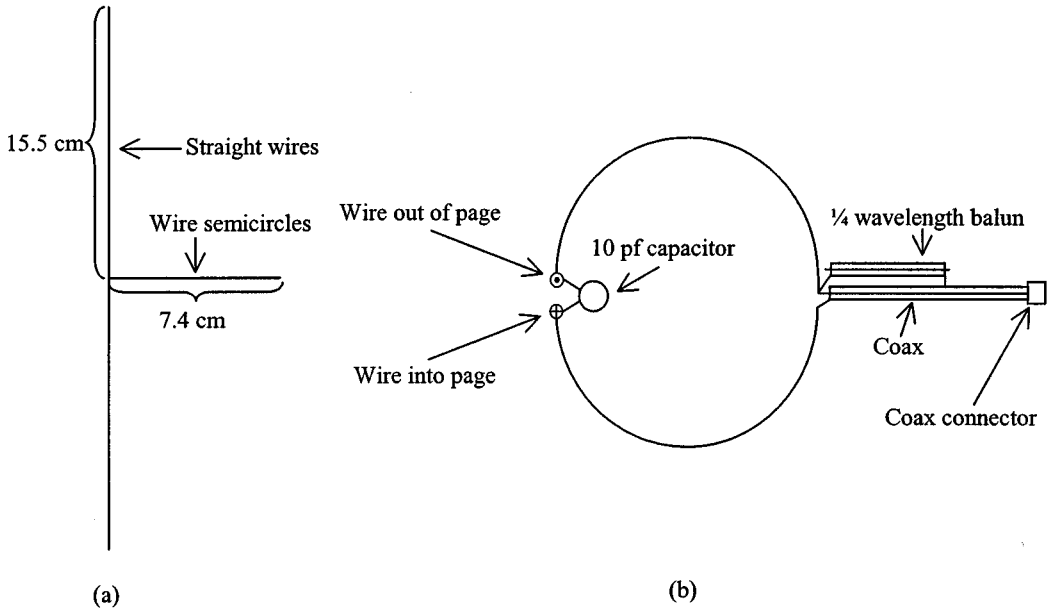

Fig. 1. Loop-dipole-capacitor (LDC) antenna design.

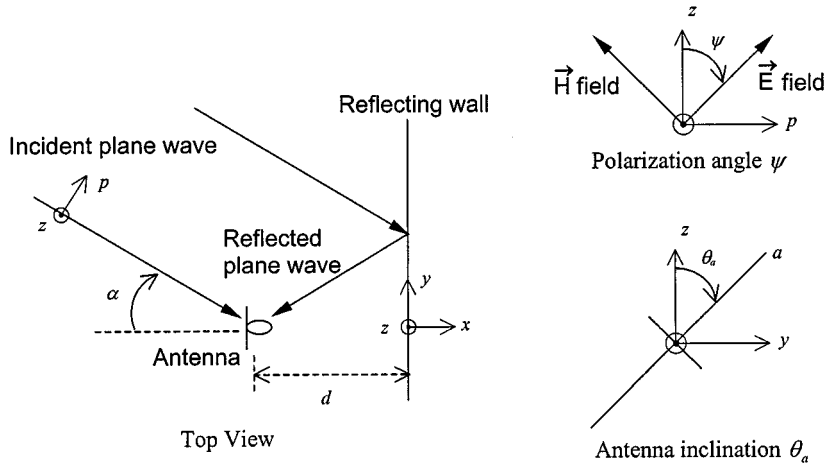

Fig. 2. Simulation and field-test geometry.

$\pi/4$. This is supported by results in Section II-A, which show that substantial reductions in null probability occur for $\pi/8 \leq \gamma \leq \pi/2$ when a reflector is present, and for $\pi/8 \leq \gamma \leq \pi/4$ when no reflector is present.

The antenna design shown in Fig. 1 is optimized for operation at a frequency of 475 MHz, whereas typical portable transceivers (including cellular and PCS handsets) operate at frequencies between 900 and 2000 MHz. The lower operating frequency for our experimental prototype was chosen in order to avoid interference with cellular telephone signals during outdoor field tests and because test fixtures were more easily fabricated for a larger sized antenna. However, simulation studies suggest that the substantial reductions in null probabilities we observe at 475 MHz can also be realized at higher frequencies by simple geometric scaling of the design (including the capacitor), followed by slight adjustments to the relative element lengths to account for differing wire length-to-thickness ratios.

Although due to its single output port the configuration in Fig. 1 cannot be described as a diversity antenna, it is nonetheless related to several previously published designs for field and polarization diversity antennas. A dual-port loop-dipole configuration was suggested as early as 1946 [1] and was also used more recently in [2] as an automobile rooftop antenna in a polarization diversity drive-test study. Subsequently, the author of [3] pointed out that the diversity gains reported in [2], which were initially attributed primarily to polarization diversity, were also caused by elevation diversity resulting from the loop-dipole antenna's elevated position over a ground plane. An important related three-port configuration is Pierce's energy density antenna [4], where three orthogonal loops (plus a ground plane) respond to H_x, H_y, and H_z. Alternate implementations of the energy density antenna with monopole-slot combinations appear in [5]–[7] and a switched-diversity approach with two loops, intended for pager applications, is discussed in [8]. Recent papers

oriented toward hand-held transceivers, such as [9], include an analysis of the diversity gain versus antenna angle from the vertical. Reference [9] considers portable antenna design via the FDTD simulation method and studies various combinations of two antennas mounted on either side of a hand-held transceiver. Diversity gain in [9] is predicted based on far-field gain pattern measurements, under a Rayleigh assumption on the incident fields.

A unique feature of the design process described in this paper is the combined use of moment-method antenna simulations and one or more incident waves or incident/reflected wave pairs. The moment-method gives far-field gain patterns, which are then used to predict antenna performance in the presence of a fixed reflector by superimposing responses to incident and reflected waves. This approach uses different assumptions about the antenna reception environment than those used in recent mobile antenna design papers. Specifically, we assume that in many situations a small number of dominant paths determine the electromagnetic field environment at the portable transceiver. For each of these, the incident and reflected waves are related by boundary conditions on nearby reflectors. This contrasts with the commonly used assumption of a Rayleigh distributed incident field [8]–[11]. The approach used here is specifically intended for multi-element antenna design in that all necessary field components are computed in order to predict the magnitude and phase of the antenna response. By contrast, previous multipath studies [15]–[17] are focused primarily on either predicting antenna coverage patterns or on spatial diversity reception and generally give only the power of the E_z component ([15], however, does predict several more detailed properties of the multipath channel from a ray-tracing simulation, including the total received power in the vertical and horizontal E-field components). We also note that the present version of our simulation permits only a single reflector, whereas [15]–[17] permit multiple rectangular reflectors aligned in typical indoor office or outdoor city-block configurations. Finally, we note that analysis of diversity antenna performance in the presence of a reflecting plane was considered in [5]; however, that work did not allow for an arbitrary polarization of the received field, and derived only bounds on the signal amplitudes, as opposed to the cumulative distribution functions (cdfs) that are both derived theoretically and measured experimentally in this paper.

To summarize, the key contributions of this paper are: 1) a new two-element antenna design for portable transceivers featuring passive combining and a single feedpoint, which exploits known phase relationships between the incident E and H fields in a multipath environment in order to reduce the probability of deep fades in the received signal; 2) a new approach to simulating antenna performance in multipath environments, using antenna gain-pattern simulation together with superposition of incident fields near a fixed reflector to derive cdfs of the received signal envelope under random variations of incidence angle, distance from reflector, antenna inclination, and field polarization; and 3) field measurements of antenna performance that confirm the results predicted by simulation.

The rest of the paper is organized as follows. Section II compares the assumptions used in the present antenna design to the more commonly used Rayleigh assumptions. Section II also presents theoretical results that motivate the design. Section III presents details of the simulation environment used to optimize the design and Section IV summarizes the experimental set up for the field tests. Section V provides simulation results and field test measurements for three contrasting antenna designs: a dipole, a loop-dipole without capacitor (referred to as the LD antenna) and the loop-dipole with capacitor shown in Fig. 1 (referred to as the LDC antenna). Section VI presents conclusions. The Appendix provides a derivation of the cumulative distribution function of the LDC antenna in the reflecting plane environment.

II. Dominant Path Model and Design Considerations

The design assumptions in this paper reflect the fact that fading statistics encountered in outdoor urban or suburban environments are frequently not Rayleigh [10], [12]–[14]. A suggested explanation for this fact is that the number of multipath components may not be high enough to yield Rayleigh statistics at the portable transceiver. Table I compares two sets of assumptions about the transceiver's reception environment: the *dominant path model*, used in our simulations and field tests, and the *continuous source Rayleigh model*, used in recent papers on diversity antenna design [9], [10]. The continuous source Rayleigh model is a statistical method for describing the multipath environment at the transceiver and works very well when there are a large number of uncorrelated incident waves.

However, when only a small number of paths exist, it is possible to improve upon designs based on Rayleigh assumptions by taking into account known phase relationships between the electric and magnetic fields. This point is mentioned in [10], where it is pointed out that two antennas receiving signals 90° apart in phase can almost completely eliminate the effects of fading. In this case, the envelope correlation coefficient ρ_e between the two antenna voltages is -0.92, a result inconsistent with the Rayleigh assumption, which implies $\rho_e \geq 0$. Field measurements of ρ_e frequently turn out to be negative [10], [13], [14], a fact that motivates our attempt to define a more realistic set of modeling assumptions.

A. Theoretical Cumulative Distribution Function of the LDC Antenna

The capacitor in Fig. 1 introduces a phase shift γ between the voltages on the loop and dipole elements. For the geometry of Fig. 2, under the assumptions of perfect reflection from the yz plane and a single vertically polarized incident plane wave (i.e., $\psi = 0$), the field components E_a and H_a along the a axis are

$$E_a = -2jE_0 \cos\theta_a \sin(k_0\, d \cos\alpha) \exp[j(\omega t + \zeta)] \quad (3)$$

$$H_a = -2\frac{E_0}{\eta_0} \sin\theta_a \cos(k_0\, d \cos\alpha) \exp[j(\omega t + \zeta)] \quad (4)$$

where ζ is an arbitrary phase. We now consider the series combination of voltages from loop and dipole and show that the optimum value for γ when the antenna response is averaged over inclination θ_a and distance d is $\pi/2$. The voltage magnitude V

TABLE I
MULTIPATH MODEL COMPARISON

Name of model	Dominant Path	Continuous source Rayleigh
Number of incident waves	< 5	∞
Fading envelope density	Non-Rayleigh	Rayleigh
Spatial distribution of sources	Discrete point sources	Continuous
Vertical direction of arrival	Horizontal plane	Horizontal plane
Horizontal direction of arrival	Angles α_i independent for each ray	Constant time averaged power density per steradian
Polarization	Polarization angles ψ_i independent for each ray, and independent of α_i	1. Uncorrelated orthogonal polarizations 2. Polarizations are spatially uncorrelated
Reflector configuration	Shown in Figure 2	Not applicable
Statistical antenna gain	Based on the received envelope c.d.f. computed over a range of incidence and polarization angles, and distances from reflector, with antenna gain pattern taken into account	Based on the received envelope c.d.f. computed from continuous source Rayleigh assumptions, and antenna gain pattern

from the series combination is given by (1). Without loss of generality we set the gain constant $C = 1/E_0$ so that V ranges between 0–2 V. Then after some manipulation, we obtain

$$V = \sqrt{2}\left[1 - \tfrac{1}{2}(1-\cos\gamma)\cos(2\theta_a - 2\xi) - \tfrac{1}{2}(1+\cos\gamma)\cos(2\theta_a + 2\xi)\right]^{1/2} \quad (5)$$

where $\xi = k_0 d\cos\alpha$. To evaluate average antenna performance, we assume that θ_a and ξ are independent and uniformly distributed between $-\pi$ and π. This models the case where α is fixed and θ_a and d are unknown. Under these conditions, it is shown in the Appendix that the probability density function (pdf) of V is

$$f_V(v) = \begin{cases} \dfrac{2v}{\pi^2\sqrt{1-\cos^2\gamma}} K\left(\sqrt{\dfrac{v^2(1-(v/2)^2)}{1-\cos^2\gamma}}\right) \\ \qquad 0 < v < \sqrt{2(1-\cos\gamma)} \\ +\infty, \qquad v = \sqrt{2(1-\cos\gamma)} \\ \dfrac{2v}{\pi^2\sqrt{v^2(1-(v/2)^2)}} K\left(\sqrt{\dfrac{1-\cos^2\gamma}{v^2(1-(v/2)^2)}}\right) \\ \qquad \sqrt{2(1-\cos\gamma)} < v < \sqrt{2(1+\cos\gamma)} \\ +\infty, \qquad v = \sqrt{2(1+\cos\gamma)} \\ \dfrac{2v}{\pi^2\sqrt{1-\cos^2\gamma}} K\left(\sqrt{\dfrac{v^2(1-(v/2)^2)}{1-\cos^2\gamma}}\right) \\ \qquad \sqrt{2(1+\cos\gamma)} < v < 2 \end{cases} \quad (6)$$

where $K(\cdot)$ denotes the complete elliptic integral, i.e., $K(k) = \int_0^1 [(1-x^2)(1-k^2x^2)]^{-1/2}\,dx$. In general, $f_V(v)$ has two singularities. However, for $\gamma = 0$ only the third and fourth cases of (6) apply, giving a single singularity at $v = 2$, while for $\gamma = \pi/2$, only the first, second, and last cases apply, giving a single singularity at $v = \sqrt{2}$. Also, $\lim_{v\to 0} f_V(v) = 0$ for all γ except $\gamma = 0$, where the limit is $1/\pi$. Hence, *any nonzero phase shift γ will significantly reduce the probability of deep fades compared to the case $\gamma = 0$.* By contrast, a dipole receiving only the E_a field (3) has pdf

$$f_{V_{\text{dipole}}}(v) = \frac{2}{\pi^2} K\left(\sqrt{1-(v/2)^2}\right), \qquad 0 < v < 2. \quad (7)$$

The dipole pdf has a single singularity at $v = 0$, which significantly increases its fading probability compared to the LDC antenna.

Fig. 3 shows cdfs $F_V(v)$ for the LDC and dipole antennas, computed by numerical integration of (6) and (7). The figure shows that phase shift $\gamma = \pi/2$ provides the greatest reduction in null probability. For example, the probability of a signal fade 26 dB or more below maximum is about $10^{-1.2}$ for the dipole, but only about $10^{-2.9}$ for the LDC, a reduction of almost two orders of magnitude. Alternatively, at a fixed fading probability of $10^{-1.8}$, the LDC with $\gamma = \pi/2$ provides about 32 dB of gain over the dipole and even the relatively small phase shift of $\gamma = \pi/8$ realizes most (27 dB) of the available gain.

We have also computed the theoretical pdf $f_{V_{\text{free}}}(v)$ of the LDC antenna in free-space (without reflector), assuming a single-incident plane wave, with inclination angle $\theta_a$uniformly distributed between $-\pi$ and π

$$f_{V_{\text{free}}}(v) = 2v\left[\pi|\sin\gamma|\sqrt{1-\left(\frac{1-v^2}{\sin\gamma}\right)^2}\right]^{-1} \qquad \sqrt{1-|\sin\gamma|} < v < \sqrt{1+|\sin\gamma|}. \quad (8)$$

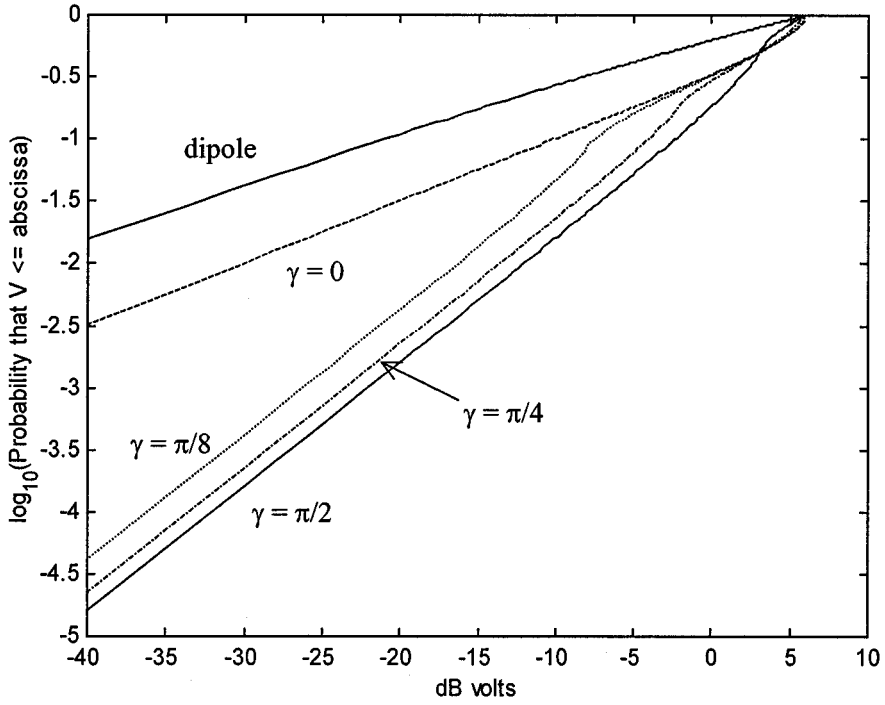

Fig. 3. Theoretical cdf of received voltage magnitude V from the LDC antenna in the vicinity of a reflecting wall, for various values of the capacitor-induced phase shift γ. The cdf of the dipole antenna is also shown for comparison.

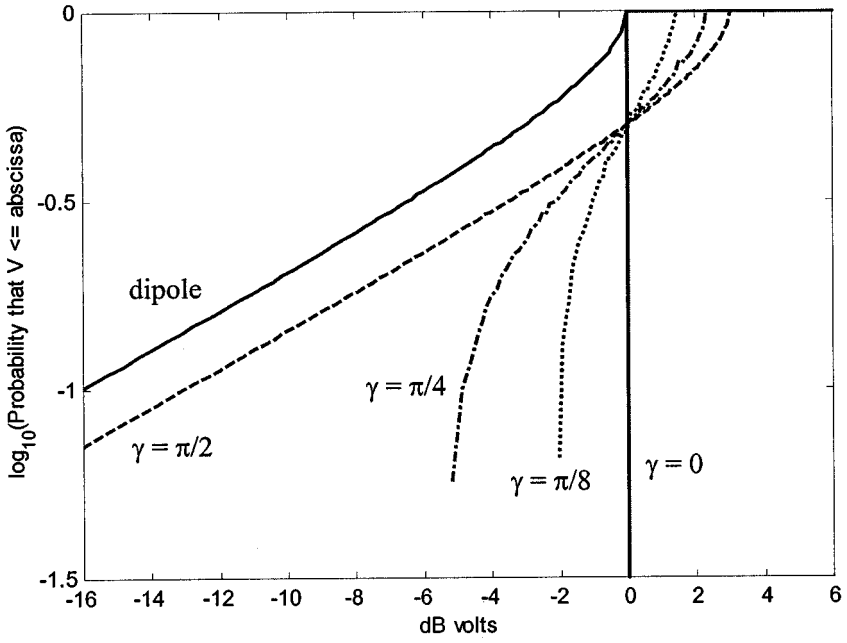

Fig. 4. Theoretical cdf of received voltage magnitude V from the LDC antenna in free-space for various values of the capacitor-induced phase shift γ.

Fig. 4 shows the cdf corresponding to $f_{V_{\text{free}}}(v)$. Although a value of $\gamma = 0$ makes the antenna response invariant to θ_a, values $\gamma = \pi/8$ and $\gamma = \pi/4$ still achieve most of the available gain over the dipole. We conclude that choosing $\pi/8 \leq \gamma \leq \pi/4$ gives the best overall performance for the LDC antenna, with or without the reflector.

III. Simulation Environment

The simulation environment consists of two separate simulations. An antenna is first designed using Mininec Professional for Windows [18]. Mininec is a moment-method program applicable to thin-wire antennas with the capability of

including lumped elements, as required by our LDC antenna. From Mininec, far-field amplitude and phase relationships are obtained and used as parameters in a multipath simulation.

The multipath simulation assumes one or more incident plane waves and a reflecting surface. The reflector consists of a perfectly conducting yz-plane (Fig. 2). As such, the tangential E-fields at the surface must be zero and the reflection coefficients are $\Gamma_{||} = 1$ and $\Gamma_{\perp} = -1$. $\Gamma_{||}$ is the coefficient for the E-field parallel to the plane created by the propagation vector and the surface normal and $\Gamma_{\perp}$ is for the E-field perpendicular to the same plane [19].

The incident Poynting vectors are assumed to lie in the xy-plane. Except for the reflector, the simulation assumes free-space; in particular, the xy-plane is *not* treated as a ground plane. These assumptions eliminate ground reflections and eliminate effects due to the antenna's elevation pattern. The necessity of eliminating elevation pattern effects when studying antenna response to polarization alone has been noted previously in [3]. In our case, we study the antenna's response to multiple incident waves with independent polarization and incidence angles under the assumptions listed in Table I.

The multipath simulation allows independent randomization of each incident wave's polarization and incidence angles, and of the distance of the antenna under test (AUT) from the reflector. All three parameters may also be set as constants, or uniformly stepped through a range of values. The number of incident waves may also be varied. An operating frequency is specified to calculate phase changes due to the reflector and movement of the antenna.

The E- and H-fields at the AUT are calculated by summing the incident and reflected plane waves. Equations for the field components received by a z-oriented antenna (i.e., $\theta_a = 0$) for a single incident/reflected wave pair are as follows:

$$E_a = E_z = \cos\psi(E_\theta^i e^{-jk_0 x\cos\alpha} + E_\theta^r \Gamma_\perp e^{jk_0 x\cos\alpha}) \quad (9)$$

$$H_a = H_z = \sin\psi(E_\phi^i e^{-jk_0 x\cos\alpha} + E_\phi^r \Gamma_{||} e^{jk_0 x\cos\alpha}). \quad (10)$$

E_ϕ^i, E_θ^i, and E_ϕ^r, E_θ^r are the far-field complex gain coefficients corresponding to the incident and reflected paths and are computed in the Mininec simulation.

By incorporating the gain coefficients into the multipath simulation, the correct complex constants of proportionality between $V_{\text{dipole}} \propto E_z$ and $V_{\text{loop}} \propto H_z$ are included and thus, V_{out} for the simulated loop-dipole configurations is found by

$$V_{\text{out}} = E_z + \eta_0 H_z \quad (11)$$

where E_z and H_z are given in (9) and (10), respectively. V_{out} for the simulated dipole antenna response is simply equal to E_z.

To simulate the field test cases presented in this paper, the AUT is oriented with the dipole element parallel with the z-axis (i.e., $\theta_a = 0$) and one incident plane wave is specified. The wave's E-field polarization is set at $\psi = 45°$, while incidence angle α varies randomly from -45 to $45°$ and the distance d varies randomly from 0.124 to 0.524 m and is independent of α. One million trials are run and the data is collected in the form of a histogram and converted to a pdf. The simulation results are presented in Section V below.

IV. Field Test Configuration

Verification of the simulation results was performed on the antenna test range at Larsen Electronics, Vancouver, WA. In the test configuration (Fig. 5), an aluminum reflector screen with a width of 3.76 m and a height of 1.85 m was mounted on a turnstile, perpendicular to an asphalt surface. A movable wooden arm, parallel to the ground, and attached to the turnstile, extended a short distance in front of the screen for mounting the AUT. A dipole source antenna was placed above the center of an asphalt surface 5.82 m from the screen when the turnstile was in the $0°$ position. The dipole source was oriented vertically while the AUT was rotated $45°$ from vertical; this arrangement preserved the simulation environment's $45°$ angle between the incident E-field and the dipole axis a. The fixed angle of $45°$ was chosen to limit the experiments to within our allotted test range time, and because $45°$ is a typical vertical inclination angle when hand-held transceivers are used in the field.

Before evaluating the experimental setup, the main object of the work should be reviewed. Of most interest here is the suppression of nulls due to interference between incident and reflected plane waves at various field points, angles of incidence, and AUT orientations. Hence, the absolute amplitude of the incident wave and the absolute response of the AUT were relevant only to ensure a detectable signal and sufficient dynamic range for null measurements. What is important is that the incident wave arrives in a horizontal plane and has approximately constant amplitude and that the environment of the AUT consists of incident and reflected plane waves of roughly equal amplitude over the set of parameters varied during the experiment.

The turnstile/screen had a radius of 3.44 m, so the exact distance from the source antenna to the screen's center (and, hence, the incident wave amplitude) varied as the turnstile rotated. However, this was considered negligible since, as mentioned above, the most important field characteristics at the AUT were the relative phase and amplitude of the incident and reflected waves. The turnstile radius did cause some difference in the incidence angle; for a $30°$ turnstile angle, the angle of incidence with respect to the normal of the screen was actually approximately $45°$. Therefore, the data collected for turnstile angles of -30 to $30°$ was compared to simulation data for $\alpha = -45$ to $45°$.

In the experiment, the centers of both the AUT and the dipole source were placed 16 cm (about 0.25 wavelengths) above the asphalt surface. The asphalt was assumed to have a dielectric constant of 2.68 and a conductivity of zero [20]. The antennas were placed near the ground to eliminate interference nulls due to ground reflections, and to ensure that all waves (including ground reflections) arrived at the AUT in the horizontal plane, thereby eliminating effects due to the antenna's elevation pattern (see, e.g., [3], where it is shown that little or no elevation pattern decorrelation of loop and dipole envelope voltages occurs if their heights above a ground plane are less than or equal to 0.25 λ). The incidence angles of the ground reflected rays varied between $2.85°$ and $3.46°$; the minimum occurred when

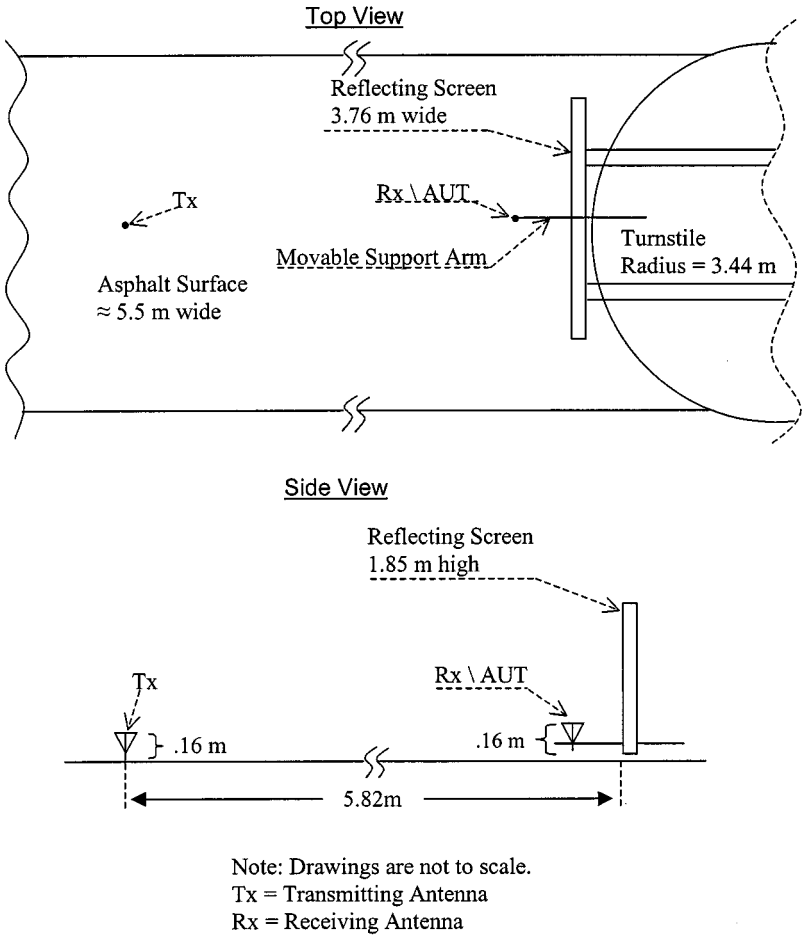

Fig. 5. Field test setup at Larsen Electronics.

the turnstile was at 30° and when d was 0.124 m. At these angles of incidence, the ground reflection coefficient $\Gamma_{\|}$ for vertically polarized waves is about -0.80 and the antenna response (to first order) is equal to the response from the nonground waves times a path gain F that accounts for the ground wave interference [21, p. 341–46]. In our case, when the turnstile is at 0°, F is about 0.21 for both the direct and reflected paths and varies by no more than $\pm 5\%$ as d varies over its full range. The specific value of F is not important as long as its variation with d is small, because the experimental objective was to examine the relative response of the AUT to different incident/reflected wave pairs.

Since the direct line of sight path between the source dipole and the AUT was only 0.16 m above the asphalt and the reflected wave was assumed to be a plane wave for the simulations, the finite extension of the ground plane below this path must be considered. This effect is considered by first assuming (as a worst case) that the asphalt surface can be ignored and then calculating the actual field at the AUT. It can be shown using equivalence theory that the difference between a perfect reflected wave (due to an infinite reflector) and the actual reflected wave (due to a finite reflector) at any point d in front of the reflector is equal to the value of the diffracted field at a distance d behind the reflector. This diffracted field can be estimated using Fresnel diffraction theory [21]. Using an average distance d of 0.32 m, it is found that the Fresnel argument is approximately -0.52 from which the difference between the perfect and actual reflected waves is calculated to be smaller than -10 dB compared to the incident wave amplitude. Thus, while the reflector is not perfect, it is a reasonable approximation to the simulation results. A similar analysis shows the other dimensions of the reflector are large enough that diffraction can be ignored.

The foregoing discussion demonstrates that the field test configuration in Fig. 5 is roughly equivalent to the free-space simulation environment of Fig. 2, except that the source is attenuated by the path gain F. The source attenuation will not affect the shape of the measured antenna response histograms—only their absolute gain. While diffraction from the bottom of the screen is not completely negligible, the relatively good agreement we observe between the simulated and experimental pdfs Figs. 8–10 suggests that the essential features of the simulation have been captured experimentally. The deviation between measured and simulated pdfs for the LDC antenna at small signal levels could be attributed to a nonperfect reflected wave in the experiment.

The free-space equivalence of our field test setup also assumes minimal depolarization of the vertically polarized source wave by rough surface scattering. The well-known Rayleigh criterion states that surfaces with protuberances below critical height $h_c = \lambda/(8 \sin \theta_i)$, where θ_i is the incidence angle, will not exhibit rough surface scattering. In our tests, where $\theta_i \approx 3°$,

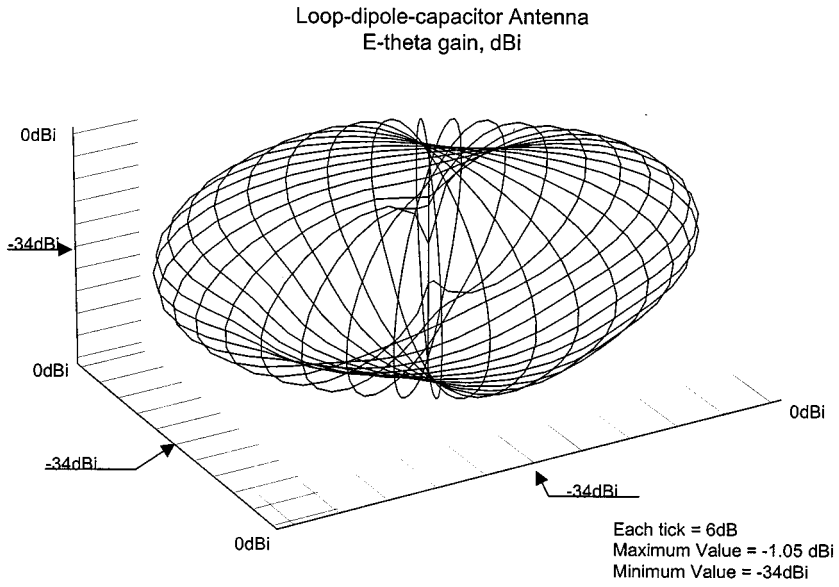

Fig. 6. Far-field gain E_θ for the LDC antenna.

the critical height $h_c \approx 1.5$ m, well above the 2–5 mm protuberances in the test-site asphalt. The lack of rough surface scattering at low incidence angles is also noted in [22], where scattering cross-section curves for slightly rough sea surfaces are presented.

The basic goal of this research was to eliminate fading problems by a simple passive combination of antenna elements. As such, no matching networks were designed for any of the antennas. To collect field test data, the source dipole was fed with a 475-MHz signal at 15 dBm from a HP8656A signal generator. An RF receiver tuned to 475 MHz and a PC data-collection system automatically recorded the AUT output signal as the turnstile rotated. For the ith antenna, where values $i = 1, 2, 3$ denote the dipole, LD, and LDC antennas, respectively, the receiver gain G_i was set at a level sufficient to record the full dynamic range of the antenna response, without saturation at the high end or loss of lock at the low end. The ith antenna's data consisted of decibel readings relative to the receiver gain G_i. Because the antennas were not matched, the receiver gains G_i were unequal. The data were obtained by setting the AUT support arm to a specific distance d from the screen and then collecting decibel readings at incidence angle increments of 0.1° as the turnstile rotated. The location of the AUT was then moved 0.02 m for another pass. A total of 21 data collection runs per antenna were completed as the distance d was stepped from 0.124–0.524 m.

V. Simulated and Field-Test Results

The three-dimensional (3-D) far-field gain patterns E_θ and E_ϕ for the LDC antenna of Fig. 1, computed by Mininec simulation, are shown in Figs. 6 and 7, respectively. The patterns are reasonably isotropic in azimuth. When the relative phase angle γ between loop and dipole voltages is exactly 90°, the LDC antenna radiates a linearly polarized E-field oriented 45° from its dipole axis; for $\gamma \neq 90°$, as is the case with the antenna in Fig. 1, the radiation is elliptically polarized.

Introducing a 90° phase shift between loop and dipole voltages in an electrically small z-oriented LDC antenna leads to 0° phase difference between E_θ and E_ϕ. In practice, nonzero lengths for the dipole and loop mean that even if a perfect 90° phase shift is achieved at their junction, the phase difference between E_θ and E_ϕ in the horizontal plane will not be exactly zero, but will vary as a function of azimuth angle around the loop. For the Fig. 1 antenna, simulation shows the far-field phase difference remains within a range of $\pm 45°$ with 63% probability, with a maximum difference of 78°. As shown in the simulation and field-test results, even this nonideal phase difference gives a performance gain well worth the slight increase in design complexity due to the capacitor.

Figs. 8–10 present pdfs of the field-test results versus the simulation. We now discuss the procedure used to find absolute gains for the simulation and experimental data. The absolute gains are needed to compare performance of the three antennas and to compare simulation and field-test results. For the simulation, the Mininec gain patterns for all three antennas are calculated with the same input power (1 W) and at the same radial distance (10 m). Although we did not design or simulate matching circuits for the tested antennas, the Mininec software automatically assumes conjugate matching of the antenna to the source when computing gain patterns. The Mininec patterns are used by the multipath simulation to generate the necessary pdf or cdf curves. Using identical input power and radial distance criterion for the gain pattern calculations allows direct comparison of the different antenna pdfs and cdfs from the multipath simulation.

For the experimental data, we assume each of the tested antennas (dipole, LD, and LDC) can be conjugate matched to the source by a passive matching network. This is always possible in theory, although in practice it may be difficult to build the matching circuit. Because the simulation pdfs are based on conjugate matched gain patterns, by normalizing (i.e., shifting) the test-data pdfs to fit the appropriate simulation pdf, a

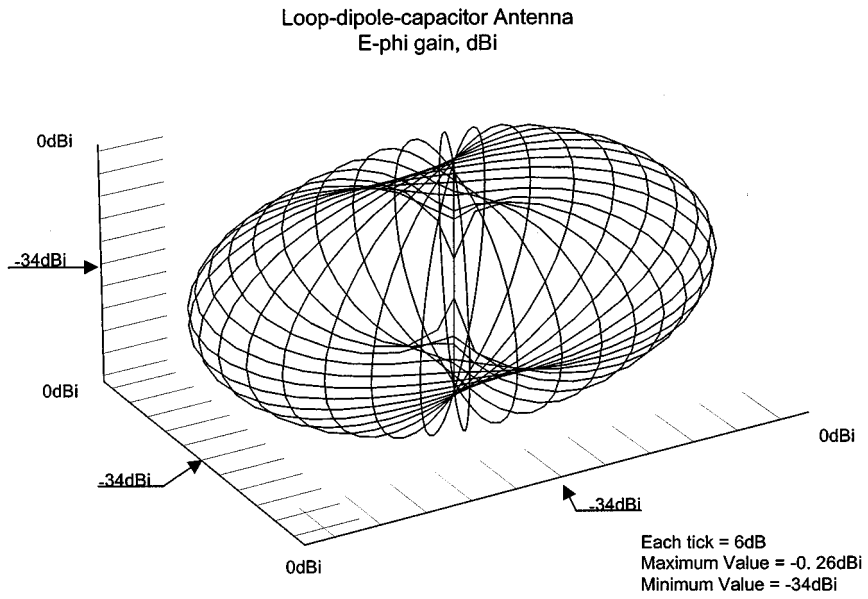

Fig. 7. Far-field gain E_ϕ for the LDC antenna.

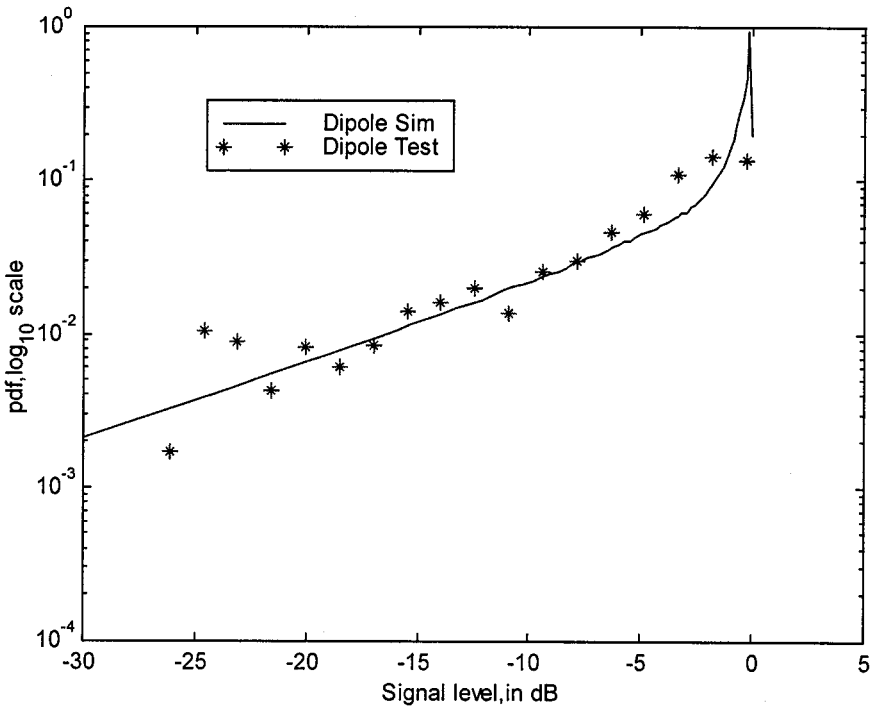

Fig. 8. Dipole pdf for $\psi = 45^\circ$, $\alpha = -45$ to 45°, and $d = 0.124$–0.524 m.

comparison between the three antennas becomes possible, even though the measured relative gains are unknown. Specifically, simulation data pdfs are created from histograms with 200 bins of width 0.015 V, with a total number of trials equal to 1 000 000. The simulation pdfs are converted to decibel volts by a probability transformation. Normalized histograms consisting of 12 600 samples with 20 bins of width 1.55 dB form the experimental pdfs. Each experimental pdf is shifted to fit the relevant simulation pdf as well as possible, under the assumption that the experimental antennas can be conjugate matched to the same overall gain predicted by the simulation.

In Figs. 8 and 9, the shapes of the experimental pdfs fit the simulation pdfs quite well, and the overall spread in test data exceeds 27 dB in both cases. In Fig. 10, the LDC test data fits the simulation curve for the region in which such curve exists with an overall test data spread of 20 dB. But more importantly, the data points below the -10 dB point fall off at a much faster rate than either the dipole or LD pdfs, indicating a significant reduction in signal fading with the LDC compared to either of the

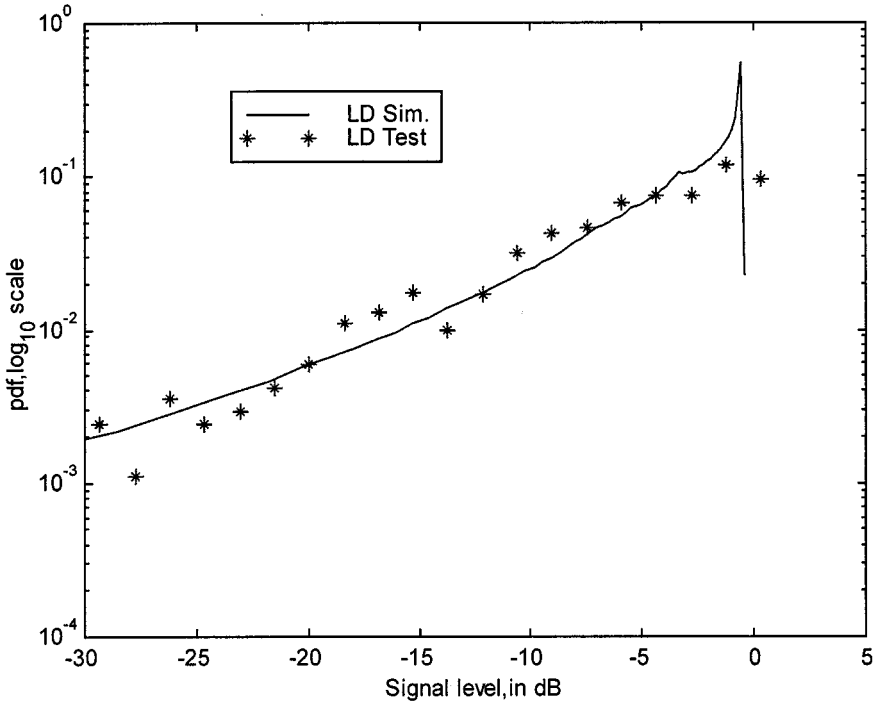

Fig. 9. LD antenna pdf for $\psi = 45°$, $\alpha = -45$ to $45°$, and $d = 0.124$–0.524 m.

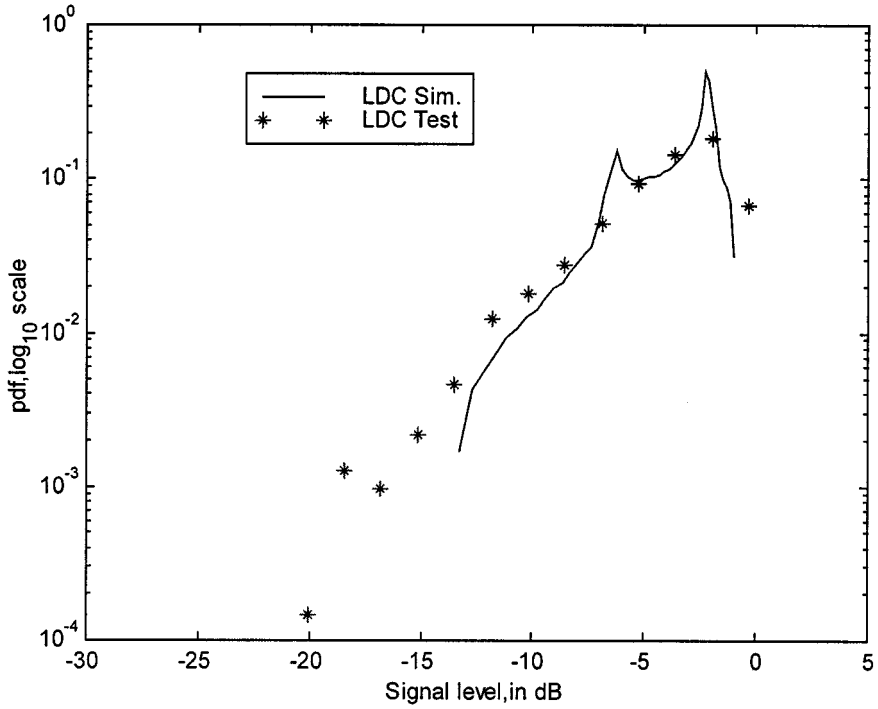

Fig. 10. LDC antenna pdf for $\psi = 45°$, $\alpha = -45$ to $45°$, and $d = 0.124$ –0.524 m.

other antennas. Fig. 11 shows the experimental cdfs, computed by numerical integration of the experimental pdfs in Figs. 8–10. In Fig. 11, the LDC exhibits approximately a two order of magnitude decrease in fading probability at the -20 dB level. Alternately, at a fixed probability of 10^{-2}, the LDC exhibits a gain in excess of 10 dB over the other antennas. These significant gains clearly illustrate the advantage of using a passive phase shifter between the antenna elements.

In further support of our method of estimating the relative gains of the experimental antennas by fitting their pdfs to the simulation pdfs, we note from the Mininec simulation that the total far-field gains of the three antennas fall within a range

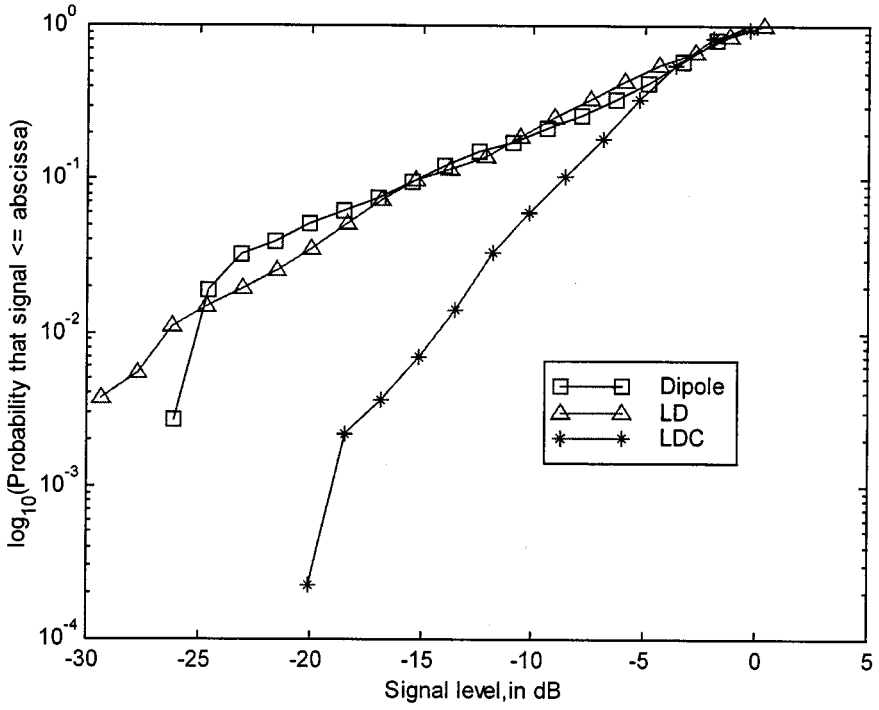

Fig. 11. cdf of test data of the three antennas.

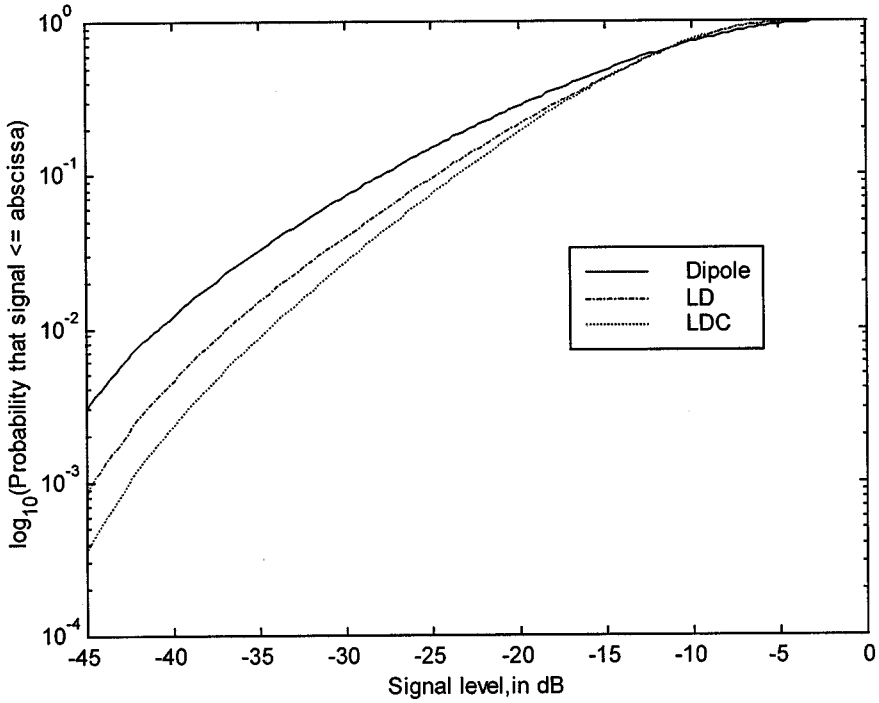

Fig. 12. Two path simulation cdf for $\alpha = -\pi/2$ to $\pi/2$, $\psi = -\pi/2$ to $\pi/2$, $\theta_\alpha = 0$, $|E| = 0$ to 1, $\angle E = -\pi$ to π, and $d = 0.100$ to 0.731m.

of 2.37 dB. This gives a worst-case gain fitting error of 2.4 dB, under the assumption of a perfect conjugate matching network for each antenna. But even if we left-shift the LDC cdf in Fig. 11 by 2.4 dB, the LDC still exhibits approximately a 7.5-dB gain over the other two antennas at fading probablity 10^{-2}. Thus, even if a worst-case absolute gain for the LDC is assumed, the very significant reduction in the probability of deep fade events exhibited by the LDC represents a distinct design advantage.

Although the experimental results are for a single incident/reflected wave pair, simulations for more than one incident wave also show cdf gains for the LDC antenna. Figs. 12 and 13 present

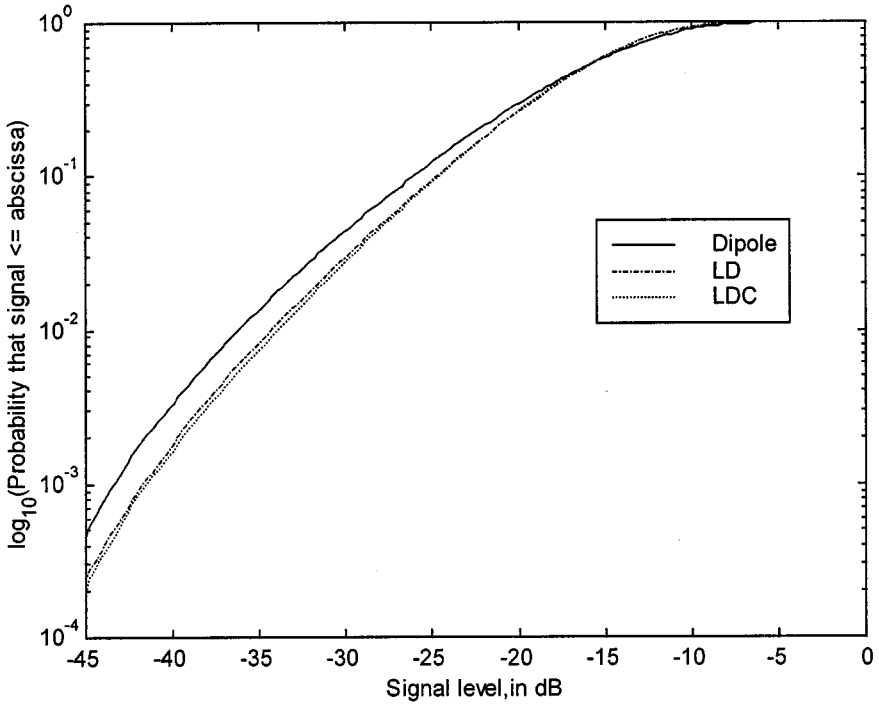

Fig. 13. Four path simulation cdf for $\alpha = -\pi/2$ to $\pi/2$, $\psi = -\pi/2$ to $\pi/2$, $\theta_a = 0$, $|E| = 0$ to 1, $\angle E = -\pi$ to π, and $d = 0.100$ to 0.731m.

simulation results for two and four incident waves, respectively, and vertical antenna inclination. These simulations use the same Mininec gain patterns as those used to produce Figs. 8–10. For each given source path, the following values are uniformly and independently distributed over the following ranges: $\alpha = -\pi/2$ to $\pi/2$, $\psi = -\pi/2$ to $\pi/2$, $d = 0.100$–0.731 meters (one wavelength), $|E| = 0$ to 1, and $\angle E = -\pi$ to π. Fig. 12 demonstrates the advantages of the phase-shifting capacitor when two dominant paths exist. Fig. 13 illustrates that, though the capacitor gives no significant advantage for four paths, it *does not deteriorate the antenna's performance*. The reduction in gain over the dipole that occurs with the increase from two to four paths is due to phasor addition of the loop and dipole outputs and would not occur if magnitude addition were used. However, magnitude addition requires an external processing circuit and power connection, whereas the antenna considered here uses no external circuitry and requires only a single feedpoint.

VI. Conclusion

This paper has considered the design of a loop-dipole-capacitor antenna for portable transceivers. The design exploits the fact that, when only a few dominant paths exist, known relationships between the incident and reflected fields can be used to reduce the probability of deep nulls in the received signal. A passive combiner removes the need for additional signal processing electronics or external power connections. The phase-shift in the combiner is optimized using design assumptions based on a dominant path plane wave model, resulting in SNR gains of 10 dB (at a fixed fading probability of 10^{-2}) over both the standard dipole antenna and over the worst-case choice of combiner phase. Antenna performance results predicted by a combined moment-method and multipath simulation are confirmed by field-test results on an outdoor test range. The experimental results in this paper are restricted to the simple case of an antenna in front of a single, perfectly reflecting wall with a single incident wave. However, simulation results from the single reflector case show that the combiner phase shift retains some performance advantage even when the number of paths is increased and that the antenna with combiner always performs at least as well as a standard dipole. Further generalizations of the dominant path design approach used in this paper, including more sophisticated ray-tracing models, more reflectors and real-world reflection coefficients, may result in improved wireless channel models and improved design methods for multi-element antennas operating in standing wave environments.

Appendix

To derive pdf $f_V(v)$ in (6), where voltage V is given in (5), define variables

$$\begin{aligned} A &= 2\theta_a - 2\xi \quad B = 2\theta_a + 2\xi \\ X &= (1+\cos\gamma)\cos B \\ Y &= (1-\cos\gamma)\cos A \\ Z &= X + Y \end{aligned} \tag{A.1}$$

so that $V = \sqrt{2 - Z}$. A simple argument, omitted here, shows that since θ_a and ξ are uniform on $(-\pi, \pi]$ and independent, then so are A and B. The symmetry of X and Y then implies that we need only consider values of γ between zero and $\pi/2$. Thus, the pdf of Z is the convolution

$$f_Z(z) = f_X(x) * f_Y(y) = G(z, l(z), u(z)) \tag{A.2}$$

where X and Y have the scaled arcsine pdfs

$$f_X(x) = \left[\pi(1+\cos\gamma)\sqrt{1-\left(\frac{x}{1+\cos\gamma}\right)^2}\right]^{-1} \quad -(1+\cos\gamma) < x < (1+\cos\gamma)$$
$$f_Y(y) = \left[\pi(1-\cos\gamma)\sqrt{1-\left(\frac{y}{1-\cos\gamma}\right)^2}\right]^{-1} \quad -(1-\cos\gamma) < y < (1-\cos\gamma) \tag{A.3}$$

and

$$G(z, l(z), u(z)) = [\pi^2(1-\cos^2\gamma)]^{-1} \int_{l(z)}^{u(z)} \left[\left(1-\left(\frac{\tau}{1+\cos\gamma}\right)^2\right)\left(1-\left(\frac{z-\tau}{1-\cos\gamma}\right)^2\right)\right]^{-1/2} d\tau. \tag{A.4}$$

The support region of $f_Z(z)$ is $-2 < z < 2$. The pdfs in (A.3) are zero outside the indicated support regions. The upper and lower limits (l, u) in (A.4), which range over the support region of the integrand, vary with z as follows:

$$(l(z), u(z)) = \begin{cases} (-1-\cos\gamma, \\ \quad 1-\cos\gamma+z), & -2 < z < -2\cos\gamma \\ (-1+\cos\gamma+z, \\ \quad 1-\cos\gamma+z), & -2\cos\gamma < z < 2\cos\gamma \\ (-1+\cos\gamma+z, \\ \quad 1+\cos\gamma), & 2\cos\gamma < z < 2. \end{cases} \tag{A.5}$$

We treat only the first case in (A.5), as the other cases are handled similarly. For this case, we have from (A.4) and (A.5) that

$$f_Z(z) = \frac{1}{\pi^2}\int_l^u [(-l-\tau)(u-\tau)(\tau-l)(\tau-(2z-u))]^{-1/2}\, d\tau \tag{A.6}$$

where $-l > u > l > 2z-u$. By using [23, p. 290, eq. (4), sec. 3.147], (A.6) can be written in terms of the complete elliptic integral

$$f_Z(z) = \frac{1}{\pi^2\sqrt{1-\cos^2\gamma}}\, K\left(\frac{1}{2}\sqrt{\frac{4-z^2}{1-\cos^2\gamma}}\right), \quad -2 < z < -2\cos\gamma. \tag{A.7}$$

The last case of (6) now follows from (A.7) by using $V = \sqrt{2-Z}$, and the transformation $f_V(v) = 2v f_Z(2-v^2)$. The singularities in (6) follow from the fact that $K(1) = +\infty$.

ACKNOWLEDGMENT

The authors would like to thank P. Tornatta and A. Wells, both of Larsen Electronics, Vancouver, WA, for their assistance in obtaining the field-test results reported in this paper. They would also like to thank Prof. S. Hudson, Washington State University, for useful discussions on experimental design, and Dr. J. Rockway, Naval Ocean Systems Center, San Diego, CA, for advice regarding the Mininec simulation software used in this paper. Finally, they would like to thank the anonymous reviewers for several useful suggestions.

REFERENCES

[1] A. G. Kandoian, "Three new antenna types and their applications," *Waves Electrons*, pp. 70–75, Feb. 1946.
[2] W. C.-Y. Lee and Y. S. Yeh, "Polarization diversity system for mobile radio," *IEEE Trans. Commun.*, vol. COM-20, pp. 912–923, Oct. 1972.
[3] R. G. Vaughn, "Polarization diversity in mobile communications," *IEEE Trans. Veh. Technol.*, vol. VT-39, pp. 177–186, Aug. 1990.
[4] E. N. Gilbert, "Energy reception for mobile radio," *Bell Syst. Tech. J.*, vol. 44, pp. 1779–1803, 1965.
[5] K. Itoh and D. K. Cheng, "A slot-unipole energy-density mobile antenna," *IEEE Trans. Veh. Technol.*., vol. VT-21, pp. 59–62, May 1972.
[6] J. D. Parsons, "Field-diversity antenna for U.H.F. mobile radio," *Electron. Lett.*, vol. 10, Apr. 1974.
[7] B. Halpern and P. Mayes, "The monopole slot as a two-port diversity antenna for UHF land-mobile radio systems," *IEEE Trans. Veh. Technol.*, vol. VT-33, pp. 76–83, May 1984.
[8] M. Muramoto, N. Ishii, and K. Itoh, "Characteristics of a small planar loop antenna," *IEEE Trans. Antennas Propagat.*, vol. 45, pp. 1818–1822, Dec. 1997.
[9] M. A. Jensen and Y. Rahmat-Samii, "Performance analysis of antennas for hand-held transceivers using FDTD," *IEEE Trans. Antennas Propagat.*, vol. 42, pp. 1106–1112, Aug. 1994.
[10] R. G. Vaughan and J. B. Andersen, "Antenna diversity in mobile communications," *IEEE Trans. Veh. Technol.*, vol. VT-36, pp. 149–172, Nov. 1987.
[11] W. C. Y. Lee, *Mobile Communications Design Fundamentals*, 2nd ed. New York: Wiley, 1993.
[12] R. G. Vaughan, "Signals in mobile communications: A review," *IEEE Trans. Veh. Technol.*, vol. VT-35, pp. 133–145, Nov. 1986.
[13] S. Kozono, H. Tsuruhata, and M. Sakamoto, "Base station polarization diversity reception for mobile radio," *IEEE Trans. Veh. Technol.*, vol. VT-33, pp. 301–306, Nov. 1984.
[14] A. M. D. Turkmani, A. A. Arowojolu, P. A. Jefford, and C. J. Kellet, "An experimental evaluation of the performance of two-branch space and polarization diversity schemes at 1800 MHz," *IEEE Trans. Veh. Technol.*, vol. VT-44, pp. 318–326, May 1995.
[15] H. R. Anderson, "A ray-tracing propagation model for digital broadcast systems in urban areas," *IEEE Trans. Broadcasting*, vol. 39, pp. 309–317, Sept. 1993.
[16] G. E. Corazza, V. Degli-Esposti, M. Frullone, and G. Riva, "A characterization of indoor space and frequency diversity by ray-tracing modeling," *IEEE J. Select. Areas Commun.*, vol. 14, pp. 411–419, Apr. 1996.
[17] M. A. Panjwani, A. Lynn Abbott, and T. S. Rappaport, "Interactive computation of coverage regions for wireless communication in multifloored indoor environments," *IEEE J. Select. Areas Commun.*, vol. 14, pp. 420–430, Apr. 1996.
[18] J. W. Rockway and J. C. Logan, *Mininec Professional for Windows*. Carson City, NV: EM Scientific, 1995.
[19] C. A. Balanis, *Advanced Engineering Electromagnetics*. New York: Wiley, 1989.
[20] R. C. Dorf, *The Electrical Engineering Handbook*. Boca Raton, FL: CRC, 1993.
[21] R. E. Collin, *Antennas and Radiowave Propagation*. New York: McGraw-Hill, 1985.
[22] G. R. Valenzuela, "Depolarization of EM waves by slightly rough surfaces," *IEEE Trans. Antennas Propagat.*, vol. AP-15, pp. 552–557, July 1967.
[23] I. S. Gradshteyn and I. M. Ryzhik, *Table of Integrals, Series, and Products*, 5th ed. New York: Academic, 1994.

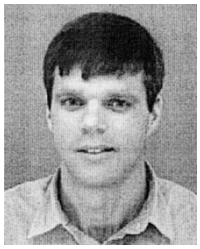

William F. Young was born in Kolonia, Ponape, on February 23, 1966. He received the B.S. degree in electronic engineering technology from Central Washington University, Ellensburg, in 1992 and the M.S. degree in electrical engineering from Washington State University, Pullman, in 1998.

He is currently a Senior Member of the Technical Staff at the Secure Communication Systems Organization, Sandia National Laboratories, Albuquerque, NM. His current work focuses on research and development in network security, particularly in ATM intrusion detection and secure network designs. Additional efforts include the development of structured approaches to network security assessments and protocol design for *ad hoc* wireless networks.

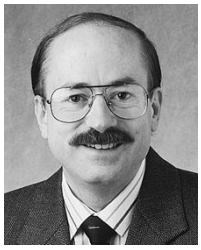

Benjamin Belzer (S'93–M'96) received the B.A. degree in physics from the University of California at San Diego, in 1982, and the Ph.D. degree in electrical engineering from the University of California at Los Angeles, in 1996.

From 1981 to 1991, he worked as a Software Engineer at Beckman Instruments, Fullerton, CA, Hughes Aircraft, Fullerton, CA, Northrop Corporation, Anaheim, CA, and Source Scientific, Garden Grove, CA, and Develco, Inc., San Jose, CA. Since 1996, he has been on the faculty of the School of Electrical Engineering and Computer Science, Washington State University, Pullman, where he is currently an Assistant Professor. His research interests include wireless communication, coding for fading channels, combined source and channel coding, and image and video communication systems.

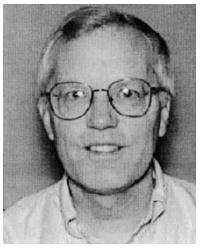

Robert G. Olsen (S'66–F'92) received the B.S. degree in electrical engineering from Rutgers University, New Brunswick, NJ, in 1968, and the M.S. and Ph.D. degrees in electrical engineering from the University of Colorado, Boulder, in 1970 and 1974, respectively.

He has been a member of the electrical engineering faculty at Washington State University, Pullman, since 1973. During that time he has been a Visiting Scientist at GTE Laboratories, Waltham, MA, at ABB Corporate Research, Västerås, Sweden, and at EPRI, Palo Alto, CA. He has also been a Visiting Professor at the Technical University of Denmark, Lyngby. His research interests include electromagnetic interference from power lines, the electromagnetic environment of power lines, electromagnetic compatibility, and electromagnetic scattering.

Dr. Olsen presently serves as Chair of the IEEE Power Engineering Society Corona Effects Fields Working Group, as Associate Editor of the IEEE TRANSACTIONS ON ELECTROMAGNETIC COMPATIBILITY, and as USNC Representative to CIGRE Study Committee 36 (electromagnetic compatibility). He is Past-Chair of the IEEE Power Engineering Society AC Fields Working Group.